

Block Encoding Linear Combinations of Pauli Strings Using the Stabilizer Formalism

Niclas Schillo^{1,2}, Andreas Sturm¹, and Rüdiger Quay^{3,4}

¹Fraunhofer-Institut für Arbeitswirtschaft und Organisation IAO, Nobelstraße 12, 70569 Stuttgart, Germany

²Universität Stuttgart, Institut für Arbeitswissenschaft und Technologiemanagement IAT, Nobelstraße 12, 70569 Stuttgart, Germany

³Fraunhofer-Institut für Angewandte Festkörperphysik IAF, Tullastraße 72, 79108 Freiburg, Germany

⁴Albert-Ludwigs-Universität Freiburg, Fritz-Hütinger Chair for Energy-Efficient High-Frequency Electronics EEH, Emmy-Noether-Straße 2, 79110 Freiburg, Germany

The Quantum Singular Value Transformation (QSVT) provides a powerful framework with the potential for quantum speedups across a wide range of applications. Its core input model is the block encoding framework, in which non-unitary matrices are embedded into larger unitary matrices. Because the gate complexity of the block-encoding subroutine largely determines the overall cost of QSVT-based algorithms, developing new and more efficient block encodings is crucial for achieving practical quantum advantage. In this paper, we introduce a novel method for constructing quantum circuits that block encode linear combinations of Pauli strings. Our approach relies on two key components. First, we apply a transformation that converts the Pauli strings into pairwise anti-commuting ones, making the transformed linear combination unitary and thus directly implementable as a quantum circuit. Second, we employ a correction transformation based on the stabilizer formalism which uses an ancilla register to restore the original Pauli strings. Our method can be implemented with an ancilla register whose size scales logarithmically with the number of Pauli strings. It can also be extended to larger ancilla registers, which can substantially reduce the overall quantum circuit complexity. We present four concrete examples and use numerical simulations to compare our method’s circuit complexity with that of the Linear Combination of Unitaries (LCU) approach. We find that our method achieves circuit complexities comparable to or better than LCU, with possible advantages when the structure of the target operators can be exploited. These results suggest that our approach could enable more efficient block encodings for a range of relevant problems extending beyond the examples analyzed in this work.

1 Introduction

Block encoding is a quantum algorithm subroutine [1, 2] that is essential for quantum algorithms such as the Quantum Eigenvalue Transformation (QET) or the Quantum Singular Value Transformation (QSVT) to solve a variety of numerical linear algebra problems

Niclas Schillo: niclas.schillo@iao.fraunhofer.de

Andreas Sturm: andreas.sturm@iao.fraunhofer.de

on quantum computers [3, 4]. At its core, block encoding allows quantum computers to perform operations with non-unitary matrices by expressing them as blocks of larger, unitary matrices with the help of ancilla qubits and post-selection. This step is crucial for many applications because quantum circuits can only implement unitary transformations, making block encoding an important link between the constraints of quantum physics and practical applications of quantum computers.

The most prominent block encoding scheme is the Linear Combination of Unitaries (LCU) method [5], which implements non-unitary operators as weighted sums of unitary matrices. Beyond the LCU approach, several other block encoding schemes have been developed to address specific matrix structures and resource constraints. These include block encoding with matrix access oracles [6–9], hardware-efficient techniques such as Hamiltonian embedding for noisy intermediate-scale quantum (NISQ) devices [10], or variational block encoding methods [11, 12] that optimize encoding parameters through classical simulation. Despite the potential quantum speedups of QSVD-based algorithms, their practical performance is often limited by the computational cost of the block encoding step that can dominate the overall resource requirements of quantum algorithms, including circuit depth, gate counts, and the number of qubits [13]. Developing explicit and efficient block encodings is therefore of central importance for advancing practical quantum algorithms.

In this work, we consider operators that are given as linear combinations of Pauli strings on n qubits with real and normalized coefficients, and with at most $2n + 1$ terms. We present a novel block encoding scheme that can implement such linear combinations of weighted Pauli strings. Our method is grounded in a key property: When a set of Pauli strings is pairwise anti-commuting and the coefficients are real and normalized, their linear combination is always unitary. This property can be very useful for different quantum algorithms, e.g., for unitary partitioning for Variational Quantum Eigensolvers (VQE) to group Pauli terms into unitary subsets [14, 15] and for efficiently constructing dressing Hamiltonians for VQE [16, 17]. Previous work also shows that using anti-commutation relations can reduce errors and gate complexity in Hamiltonian simulation algorithms [18]. The core idea of our proposed method is to leverage this property by transforming Pauli strings with commuting components into fully pairwise anti-commuting ones, allowing their linear combination to be directly implemented as a unitary operator. Subsequently, we employ a correction step, inspired by stabilizer-based quantum error correction codes [19, 20], to restore the original Pauli strings. This correction step is realized by introducing an ancilla register whose size scales logarithmically with the number of Pauli strings, constructing suitable controlled stabilizers that correlate the transformed Pauli strings with orthogonal ancilla states, and finally applying the transformation again, controlled on the ancilla states, to obtain a block encoding of the original operator. Through numerical simulations, we demonstrate that our proposed method can lead to advantages over LCU for certain examples by exploiting structure in the target operators.

Notably, our method is not limited to a logarithmic-size ancilla register and can be easily adapted to different conditions by modifying the number of ancilla qubits and the transformations. This enables a trade-off between the number of ancilla qubits and the overall quantum gate complexity. For example, we show that our method can be extended to a linear-size ancilla register which dramatically reduces the quantum gate complexity, albeit coming with a lower success probability.

This work is organized as follows: In Section 2, we introduce the notations used throughout the paper. In Section 3.1, we define the problem under consideration. Section 3.2 formally introduces the concept of block encoding. Subsequently, in Section 3.3, we outline the main idea of our proposed method, followed by a more detailed description in Section 3.4. In Sec-

tion 4, we present four concrete examples and demonstrate how they can be implemented using our proposed approach. Finally, in Section 5, we perform numerical simulations with the examples introduced before and compare the two-qubit gate count and the quantum circuit depth to LCU.

2 Notations and Conventions

In this work, we follow the standard conventions in the quantum computing literature where the Dirac notations $\langle \cdot |$ and $|\cdot \rangle$ are used to denote row and column vectors, respectively. In particular, $|0\rangle$ and $|1\rangle$ are used to denote respectively the two canonical basis vectors $(1, 0)^T$ and $(0, 1)^T$ of \mathbb{C}^2 .

For an n qubit system, we number the individual qubits as q_0, q_1, \dots, q_{n-1} . In a quantum circuit diagram we number their wires from top to bottom and we abbreviate multi-wires with a slash. For example, for $n = 3$ we have $q = q_0q_1q_2$ and

$$q \not\rightarrow = \begin{array}{c} q_0 \\ q_1 \\ q_2 \end{array} . \quad (1)$$

We denote the four Pauli matrices by

$$\sigma^{(0)} = \begin{pmatrix} 1 & 0 \\ 0 & 1 \end{pmatrix}, \quad \sigma^{(1)} = \begin{pmatrix} 0 & 1 \\ 1 & 0 \end{pmatrix}, \quad \sigma^{(2)} = \begin{pmatrix} 0 & -i \\ i & 0 \end{pmatrix}, \quad \sigma^{(3)} = \begin{pmatrix} 1 & 0 \\ 0 & -1 \end{pmatrix}. \quad (2)$$

For three different integers $a, b, c \in \{1, 2, 3\}$ they satisfy the product relation

$$\sigma^{(a)}\sigma^{(b)} = \gamma(a, b)\sigma^{(c)}, \quad \gamma(a, b) = \begin{cases} +i & \text{if } (a, b) \in \{(1, 2), (2, 3), (3, 1)\}, \\ -i & \text{if } (a, b) \in \{(2, 1), (3, 2), (1, 3)\}. \end{cases} \quad (3)$$

Two (types of) quantum gates will play a central role in this paper. Firstly, the rotational gates constructed of the Pauli matrices which we denote by

$$R\sigma^{(j)}(\theta) = \exp\left(-i\frac{\theta}{2}\sigma^{(j)}\right) = \cos\frac{\theta}{2}\sigma^{(0)} - i\sin\frac{\theta}{2}\sigma^{(j)}, \quad j \in \{1, 2, 3\}. \quad (4)$$

Secondly, the Hadamard gate given by

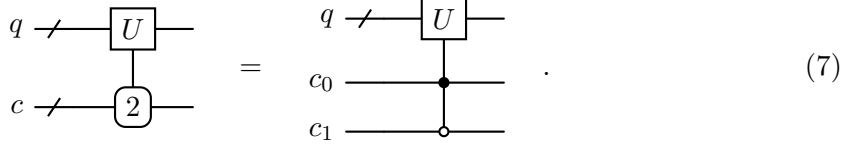
$$H = \frac{1}{\sqrt{2}} \begin{pmatrix} 1 & 1 \\ 1 & -1 \end{pmatrix}. \quad (5)$$

In the quantum circuit diagrams we will denote gates with rectangular boxes. Furthermore, we denote the controlled version of a gate U by CU and visualize it in a quantum circuit diagram as



Here, c is the control qubit and q are the target qubits. The gate U is only applied if qubit c is in the state $|1\rangle$. In a multi-qubit system, we add subscripts c and t to CU to indicate the control and target qubits. In the case of several control qubits we use round boxes

and the integer representation of the control state in the quantum circuit diagram. For example, a controlled U gate on two qubits with control state $|2\rangle = |10\rangle$ is denoted by



We indicate the qubit a quantum gate U acts on with a subscript. For example, $\sigma_i^{(j)}$ applies the Pauli gate $\sigma^{(j)}$ to the i -th qubit.

We use the term Pauli strings for tensor products of Pauli matrices

$$P = \prod_{i=0}^{n-1} \sigma_i, \quad \sigma_i \in \{\sigma_i^{(0)}, \sigma_i^{(1)}, \sigma_i^{(2)}, \sigma_i^{(3)}\}. \quad (8)$$

3 Overview of Proposed Method

In this section, we begin by formulating the operators considered in this work. We then introduce the general concept of block encoding, followed by a detailed description of our proposed block encoding scheme.

3.1 Problem Statement

In this paper, we are interested in the operator A , constructed from a weighted sum of m Pauli strings P_0, \dots, P_{m-1} ,

$$A = \sum_{k=0}^{m-1} \alpha_k P_k, \quad (9a)$$

with $m \leq 2n + 1$. Here, $\alpha_0, \dots, \alpha_{m-1}$ are real numbers that satisfy

$$\sum_{k=0}^{m-1} |\alpha_k|^2 = 1. \quad (9b)$$

Since the operator A is only unitary in special cases [14], we generally cannot apply it directly to a quantum state and must instead embed it into a larger unitary matrix.

3.2 Block Encoding

The technique of embedding a (non-unitary) matrix A into a larger unitary matrix U_A , such that

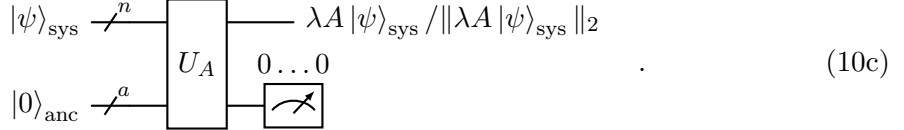
$$U_A = \lambda A \otimes |0\rangle_{\text{anc}} \langle 0|_{\text{anc}} + \sum_{(i,j) \in \{0, \dots, a-1\} \setminus \{(0,0)\}} B_{i,j} \otimes |i\rangle_{\text{anc}} \langle j|_{\text{anc}} \quad (10a)$$

is called block encoding. Here, $|\ell\rangle_{\text{anc}}$ is an ancillary system of a qubits, $B_{i,j}$ denote matrix blocks of appropriate size, whose values are irrelevant, and $\lambda \in [-1/\|A\|_2, 1/\|A\|_2]$ is a sub-normalization scaling factor that ensures $\|\lambda A\|_2 \leq 1$, which is required so that U_A exists. We use the convention that an integer i in $|i\rangle_{\text{anc}}$ refers to its binary representation as for example $|0\rangle_{\text{anc}} = |0 \dots 0\rangle_{\text{anc}}$. In the subsequence, we mark the quantum states of the

system register with $|\cdot\rangle_{\text{sys}}$ to distinguish them from the states of the ancilla register $|\cdot\rangle_{\text{anc}}$. For a composite state $|w\rangle = |\psi\rangle_{\text{sys}}|0\rangle_{\text{anc}}$ we have

$$U_A |w\rangle = \lambda A |\psi\rangle_{\text{sys}} |0\rangle_{\text{anc}} + |\perp\rangle, \quad (10b)$$

where $|\perp\rangle$ is orthogonal to $\lambda A |\psi\rangle_{\text{sys}} |0\rangle_{\text{anc}}$. This means that if we measure the ancilla qubits in the state $|0 \dots 0\rangle$, the system register contains $\lambda A |\psi\rangle_{\text{sys}} / \|\lambda A |\psi\rangle_{\text{sys}}\|_2$:



The probability to measure the ancilla system in $|0 \dots 0\rangle$ is called the success probability of the block encoding and is given by

$$p_{\text{success}} = \lambda^2 \|A |\psi\rangle_{\text{sys}}\|_2^2. \quad (10d)$$

3.3 Main Idea of Proposed Method

In this section, we describe our proposed block encoding method, which is inspired by the stabilizer measurements used in quantum error correction methods [19, 20]. We first present the core idea of our method and then elaborate on its implementation. The technical details and proofs can be found in Appendix A.

Our algorithm consists of two main parts: The first part involves transforming the generally non-unitary operator A in (9a) into a unitary operator U , by transforming the Pauli strings P_k into fully pairwise anti-commuting ones \tilde{P}_k ,

$$U = \sum_{k=0}^{m-1} \alpha_k \tilde{P}_k, \quad \tilde{P}_i \tilde{P}_j = -\tilde{P}_j \tilde{P}_i, \quad i \neq j. \quad (11)$$

The assumptions on the weights α_k in (9b) ensure that U is always unitary [14, 15]. Since the maximal number of pairwise anti-commuting Pauli strings in an n -qubit system is $2n + 1$ [21], it follows that $m \leq 2n + 1$.

The second part is to embed U into a larger system with ancillary qubits and to pre- and append operations that correct the application of U to an application of A on the system qubits. The corresponding quantum circuit is shown in Figure 1. The second part consists

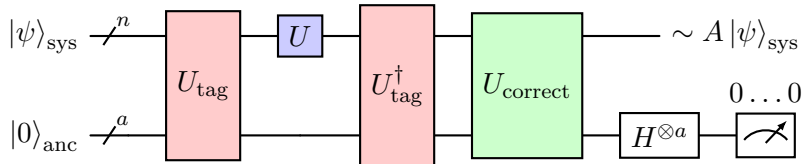


Figure 1: General quantum circuit structure of the proposed block encoding method.

of three steps. The first is the conjugation of U with a unitary operator U_{tag} that acts as

$$U_{\text{tag}}^\dagger U U_{\text{tag}} |\psi\rangle_{\text{sys}} |0\rangle_{\text{anc}} = \sum_{k=0}^{m-1} \alpha_k \tilde{P}_k |\psi\rangle_{\text{sys}} |v_k\rangle_{\text{anc}}, \quad (12)$$

where $|v_k\rangle_{\text{anc}}$ are orthogonal states of the ancilla register. This gives us control over the summands of U so that in the second step the operator U_{correct} can revert the transformation on the Pauli strings, i.e.,

$$U_{\text{correct}} \sum_{k=0}^{m-1} \alpha_k \tilde{P}_k |\psi\rangle_{\text{sys}} |v_k\rangle_{\text{anc}} = \sum_{k=0}^{m-1} \alpha_k P_k |\psi\rangle_{\text{sys}} |v_k\rangle_{\text{anc}}. \quad (13)$$

Applying Hadamard gates to all ancilla qubits as a third step gives the desired block encoding of A ,

$$(I \otimes H^{\otimes a}) \sum_{k=0}^{m-1} \alpha_k P_k |\psi\rangle_{\text{sys}} |v_k\rangle_{\text{anc}} = \frac{1}{\sqrt{2^a}} A |\psi\rangle_{\text{sys}} |0\rangle_{\text{anc}} + |\perp\rangle. \quad (14)$$

Comparing with (10) we see that the quantum circuit in Figure 1 is indeed a block encoding of A with

$$\lambda = \frac{1}{\sqrt{2^a}} \quad \text{and} \quad p_{\text{success}} = \frac{1}{2^a}. \quad (15)$$

3.4 Details of Proposed Method

Now let us present the details of the quantum circuit for our proposed block encoding, see Figure 2. Let us start with the U_{correct} operator that is composed of the controlled trans-

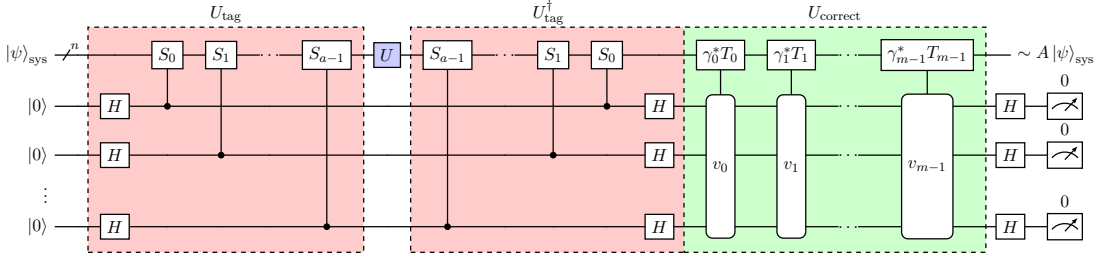


Figure 2: Detailed quantum circuit of the proposed block encoding method with an arbitrary ancilla register size.

formation operators T_0, \dots, T_{m-1} . These are pairwise commuting Pauli strings, which have to be chosen such that they transform the Pauli strings P_k under conjugation according to

$$T_i P_k T_i = \begin{cases} -P_k, & \text{if } i \leq k \text{ and } P_i P_k = P_k P_i, \\ +P_k, & \text{otherwise.} \end{cases} \quad (16)$$

Consequently, they are problem-dependent and have to be provided as input to our algorithm. Similarly, the integers $v_0, \dots, v_{m-1} \in \{0, 1, \dots, 2^a - 1\}$ have to be provided as inputs. The choice of the T_i and v_i strongly influences the quantum circuit and this freedom allows the method to be tailored to different constraints (e.g. native hardware gates or restrictions in width or depth of the quantum circuit).

Let us denote with R_k the resulting operators from applying T_k to P_k , i.e.,

$$R_k = T_k P_k, \quad k = 0, \dots, m-1. \quad (17)$$

Since both T_k and P_k are Pauli strings in the sense of (8), the operator R_k can be written as a Pauli string \tilde{P}_k and a phase factor,

$$R_k = \gamma_k \tilde{P}_k, \quad \gamma_k \in \{\pm 1, \pm i\}. \quad (18)$$

Note that the complex conjugate of γ_k appears besides the T_k operators in the quantum circuit in Figure 2. It is easy to show (see Lemma 1 in Appendix A) that the operators $\tilde{P}_0, \dots, \tilde{P}_{m-1}$ are mutually anti-commuting and thus satisfy the requirement for U in (11). As we already argued above, U is unitary.

An explicit quantum circuit for U can be constructed using a product of $2m-1$ exponentials of Pauli terms [15] as

$$U = \prod_{j=0}^{m-1} \exp\left(i\frac{\theta_j}{2}\tilde{P}_j\right) \prod_{j=m-1}^0 \exp\left(i\frac{\theta_j}{2}\tilde{P}_j\right), \quad (19a)$$

where the rotation angles θ_j are given by

$$\theta_j = \arcsin\left(\frac{\alpha_j}{\sqrt{\sum_{k=1}^j \alpha_k^2}}\right). \quad (19b)$$

The two-qubit gate count required to implement one such exponentiation scales as $\mathcal{O}(n)$ for a Pauli string acting on n qubits. Therefore, the full implementation of U requires $\mathcal{O}(mn)$ two-qubit gates. Further quantum circuit compression is possible if the Pauli strings have overlapping support or shared structure [15].

In the quantum circuit in Figure 2 we see that the operator U_{tag} consists of controlled versions of the stabilizers S_0, \dots, S_{a-1} . These are again commuting Pauli strings that have to satisfy

$$S_i \tilde{P}_k S_i = (-1)^{\Delta(2^{a-1-i}, v_k)} \tilde{P}_k, \quad (20)$$

where $\Delta(v, w)$ denotes the number of common 1-bits in the binary representation of v and w , see (43). This ensures the identity (12), which is the main statement of Theorem 1 in Appendix A. In contrary to the T_i , the S_i do not have to be provided to the algorithm, but can be computed from the T_i and v_i as we show in Lemma 3. There we also show that the S_i form a stabilizer group. In the special case that the Pauli strings P_k are fully pairwise commuting

$$P_i P_j = P_j P_i, \quad \text{for all } i, j = 0, \dots, m-1, \quad (21)$$

we provide an explicit formula to obtain the S_i from T_i and v_i in Lemma 4.

3.4.1 Choices for the Ancilla Register Size and the Control States

Exemplary choices for the number of ancilla qubits a and the control states v_0, \dots, v_{m-1} are:

- (a) Logarithmic-size ancilla register: Choose $a = \lceil \log_2 m \rceil$ and $v_k = k$.
- (b) Logarithmic-size ancilla register with Gray code sequence: Choose $a = \lceil \log_2 m \rceil$ and v_k following the Gray code sequence, which is a binary numeral system in which two successive values differ in only one bit [22].
- (c) Linear-size ancilla register: Choose $a = m$ and $v_k = 2^k$. In binary representation of v_k this means $v_k = 0 \dots 010 \dots 0$ with the 1 bit in place $m-1-k$.
- (d) Linear-size ancilla register minus one: Choose $a = m-1$ and $v_k = 1 \dots 10 \dots 0$ with k times 1 and $m-1-k$ times 0.

For the case of fully pairwise commuting Pauli strings P_k , we show the S_i for $m = 0, \dots, 14$ in Tables 2 – 4.

4 Examples

In this section, we provide specific examples of the form (9) along with possible transformations. Although our proposed method applies to general A of form (9), for simplicity, we will only focus on examples composed of pairwise commuting Pauli strings.

4.1 Example 1: Pauli Chain Operators

The simplest example considered in this work consists of Pauli strings with only one non-trivial Pauli matrix of the same type $\ell \in \{1, 2, 3\}$,

$$P_k^{(\ell)} = \sigma_k^{(\ell)}, \quad k = 0, \dots, m-1. \quad (22a)$$

Then, the weighted sum operator (9a) is given by

$$\begin{aligned} A_1^{(\ell)} &= \sum_{k=0}^{m-1} \alpha_k P_k^{(\ell)} \\ &= \alpha_0 \sigma_0^{(\ell)} + \alpha_1 \sigma_1^{(\ell)} + \alpha_2 \sigma_2^{(\ell)} + \dots + \alpha_{m-1} \sigma_{m-1}^{(\ell)}. \end{aligned} \quad (22b)$$

Despite its simplicity, such an operator occurs in many relevant problems, such as in inhomogeneous spin chains [23].

4.2 Example 2: Nearest-Neighbor Coupling Operators

Our second example is given by Pauli strings of the form

$$P_0^{(\ell)} = \sigma_{m-1}^{(\ell)} \sigma_0^{(\ell)}, \quad P_k^{(\ell)} = \sigma_{k-1}^{(\ell)} \sigma_k^{(\ell)}, \quad k = 1, \dots, m-1, \quad (23a)$$

with $\ell \in \{1, 2, 3\}$. In this case, the weighted sum of the Pauli strings results in a nearest-neighbor coupling operator given by

$$\begin{aligned} A_2^{(\ell)} &= \sum_{k=0}^{m-1} \alpha_k P_k^{(\ell)} \\ &= \alpha_0 \sigma_{m-1}^{(\ell)} \sigma_0^{(\ell)} + \alpha_1 \sigma_0^{(\ell)} \sigma_1^{(\ell)} + \alpha_2 \sigma_1^{(\ell)} \sigma_2^{(\ell)} + \dots + \alpha_{m-1} \sigma_{m-2}^{(\ell)} \sigma_{m-1}^{(\ell)}. \end{aligned} \quad (23b)$$

This operator also appears in relevant systems such as inhomogeneous spin chains.

4.3 Example 3: Pauli Staircase Operators

In our next example, we consider Pauli strings with only a single Pauli matrix type $\ell \in \{1, 2, 3\}$ that form a staircase

$$P_k^{(\ell)} = \prod_{i=0}^k \sigma_i^{(\ell)}, \quad k = 0, \dots, m-1. \quad (24a)$$

The resulting sum takes the form

$$\begin{aligned} A_3^{(\ell)} &= \sum_{k=0}^{m-1} \alpha_k P_k^{(\ell)} \\ &= \alpha_0 \sigma_0^{(\ell)} + \alpha_1 \sigma_0^{(\ell)} \sigma_1^{(\ell)} + \alpha_2 \sigma_0^{(\ell)} \sigma_1^{(\ell)} \sigma_2^{(\ell)} + \dots + \alpha_{m-1} \sigma_0^{(\ell)} \sigma_1^{(\ell)} \sigma_2^{(\ell)} \dots \sigma_{m-1}^{(\ell)}. \end{aligned} \quad (24b)$$

We include this example because it has a greater Pauli weight compared to the other examples.

4.4 Example 4: Linear Combination of Pauli Chain Operators

For our last example, we consider a slightly more general situation. Let $\ell_1, \ell_2 \in \{1, 2, 3\}$ with $\ell_1 \neq \ell_2$. Consider $A_1^{(\ell_1)}$ and $A_1^{(\ell_2)}$ constructed according to (22b) with coefficients $\alpha_k^{(1)}$ and $\alpha_k^{(2)}$, respectively. Then, we define

$$A_4^{(\ell_1, \ell_2)} = \beta A_1^{(\ell_1)} + (1 - \beta) A_1^{(\ell_2)}, \quad (25)$$

with a real coefficient $\beta \in [0, 1]$.

4.5 Transformations

Next, we present possible transformations for the examples presented above. Clearly, this is only one possible choice, but the presented configuration has the advantage that the resulting U operators take the form

$$U^{(a,b)} = \sum_{k=0}^{m-1} \alpha_k \tilde{P}_k^{(a,b)}, \quad (26a)$$

with

$$\tilde{P}_0^{(a,b)} = \sigma_0^{(b)}, \quad \tilde{P}_k^{(a,b)} = \left(\prod_{i=0}^{k-1} \sigma_i^{(a)} \right) \sigma_k^{(b)}, \quad k = 1, \dots, m-1, \quad (26b)$$

for all examples. These unitaries can be directly implemented as a quantum circuit, as shown in Appendix C.

4.5.1 Transformations for Example 1

Let $s \in \{1, 2, 3\} \setminus \{\ell\}$. Then, one possible set of transformation operators $T_k^{(s)}$ is given by

$$T_k^{(s)} = \prod_{i=0}^{k-1} \sigma_i^{(s)}, \quad k = 1, \dots, m-1, \quad (27)$$

and $T_0^{(s)} = I$, where we denote with $I = \prod_{i=0}^{n-1} \sigma_i^{(0)}$ the identity operator on all qubits. This transformation leads to

$$R_0^{(s,\ell)} = \sigma_0^{(\ell)}, \quad R_k^{(s,\ell)} = T_k^{(s)} P_k^{(\ell)} = \left(\prod_{i=0}^{k-1} \sigma_i^{(s)} \right) \sigma_k^{(\ell)}, \quad k = 1, \dots, m-1, \quad (28)$$

and the resulting unitary operator U_1 takes the form (26a), with $a = s$ and $b = \ell$.

4.5.2 Transformations for Example 2

Let $s \in \{1, 2, 3\} \setminus \{\ell\}$ and $r \in \{1, 2, 3\} \setminus \{\ell, s\}$. A possible set of transformation operators $T_k^{(s,r)}$ consists of choosing

$$T_k^{(s,r)} = \left(\prod_{i=0}^{k-2} \sigma_i^{(s)} \right) \sigma_{k-1}^{(r)}, \quad k = 2, \dots, m-1, \quad (29)$$

together with $T_0^{(s,r)} = \sigma_{m-1}^{(\ell)}$ and $T_1^{(s,r)} = \sigma_0^{(r)}$. Using (3), we see that this transformation leads to

$$R_k^{(s,r,\ell)} = T_k^{(s,r)} P_k^{(\ell)} = \gamma(r, \ell) \left(\prod_{i=0}^{k-1} \sigma_i^{(s)} \right) \sigma_k^{(\ell)}, \quad k = 1, \dots, m-1, \quad (30)$$

and $R_0^{(s,\ell,r)} = \sigma_0^{(\ell)}$. Again, the unitary operator U_2 takes the form (26a) with $a = s$ and $b = \ell$.

4.5.3 Transformations for Example 3

Again, let $s \in \{1, 2, 3\} \setminus \{\ell\}$ and let the transformation operators $T_k^{(s)}$ be given by

$$T_k^{(s)} = \sigma_k^{(s)}. \quad (31)$$

Then, we obtain

$$R_k^{(s,\ell)} = T_k^{(s)} P_k^{(\ell)} = \gamma(s, \ell) \left(\prod_{i=0}^{k-1} \sigma_i^{(\ell)} \right) \sigma_k^{(r)}, \quad (32)$$

where r is defined via $r \in \{1, 2, 3\} \setminus \{s, \ell\}$ so that (3) is satisfied. The unitary operator U_3 takes the form (26a) with $a = \ell$ and $b = r$.

4.5.4 Transformations for Example 4

For our last example, we choose $s \in \{1, 2, 3\} \setminus \{\ell_1, \ell_2\}$. Then, the same transformation operators $T_k^{(s)}$ as given in (27) can be used for $A_1^{(\ell_1)}$ and $A_1^{(\ell_2)}$. As a consequence U_{tag} and U_{correct} are also the same, so that

$$U_4^{(s, \ell_1, \ell_2)} = \beta U_1^{(s, \ell_1)} + (1 - \beta) U_1^{(s, \ell_2)}, \quad (33)$$

can be implemented with the quantum circuit in Figure 3 with

$$\phi = 2 \arccos \beta. \quad (34)$$

This optimization simplifies the quantum circuit structure and reduces the number of required quantum operations. As seen in the numerical simulations in Section 5.1, reusing the unitaries U_{tag} and U_{correct} reduces the overall circuit complexity compared to a standard LCU implementation. For simplicity, the coefficient β was chosen to be real. By using a general state preparation, complex coefficients are also possible.

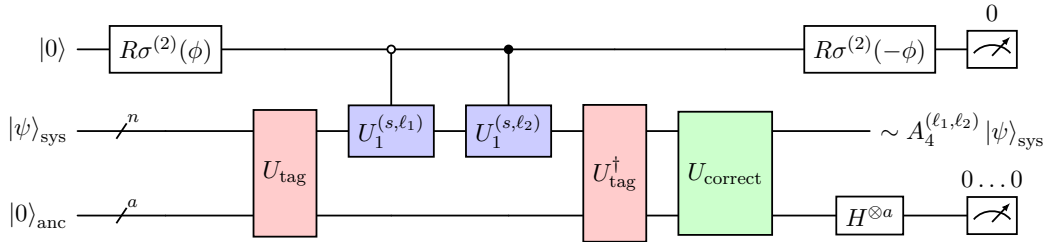


Figure 3: Quantum circuit for the block encoding of operator A_4 combining our proposed method with an additional LCU step.

5 Numerical Comparison

In this section, we compare the quantum resource requirements between the LCU method [5] and our proposed stabilizer-based block encoding for the examples in Section 4. For an adequate comparison, both methods are implemented with Qiskit [24]. The coefficients α_i (and β) are chosen randomly for all examples.

5.1 Logarithmic Ancilla Register

First, we consider the case where both the LCU and our proposed block encoding use a logarithmic-sized ancilla register. Moreover, we use the Gray code sequence for the v_k in our proposed method.

5.1.1 Block Encoding of Operators A_1, A_2 , and A_3

For the examples $A_1^{(1)}, A_2^{(1)}$, and $A_3^{(1)}$ we use the quantum circuit in Figure 2 with transformation operators T_k , phases γ_k , and unitary U as presented in Sections 4.5.1 – 4.5.3. The stabilizers S_k are constructed via (65). In Figure 4, we plot the total number of two-qubit gates and the quantum circuit depth of the block encoding via the LCU method (circular markers) and our proposed approach (triangular markers). We note that we simplified the implementation of LCU and our proposed method, using CNOT fan-out (see Appendix D). The plots show that for all three examples the scaling of our method is similar to that of the LCU approach. The overall quantum circuit depth remains very similar, while our method incurs a slightly higher two-qubit gate count. This slight overhead arises primarily from the implementation of U_{tag} . However, U_{tag} has a low Pauli weight and its implementation can be largely parallelized, which results in the impact on the quantum circuit depth being less pronounced.

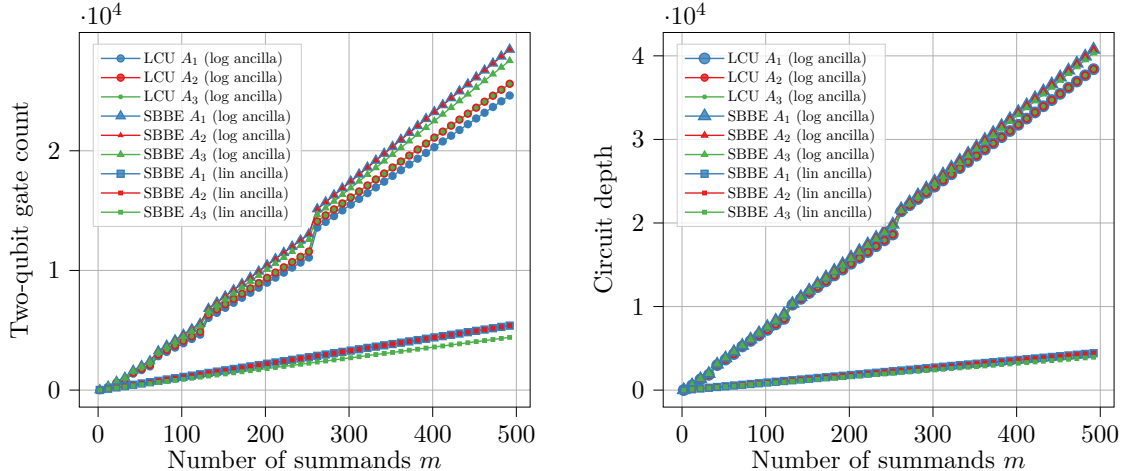


Figure 4: Numerical comparison of two-qubit gate count and quantum circuit depth for the block encoding of $A_1^{(1)}, A_2^{(1)}$, and $A_3^{(1)}$ using the standard LCU approach with $a = \lceil \log_2 m \rceil$ (circular markers) and our proposed stabilizer-based block encoding (SBBE) approach. Our proposed method is implemented with a logarithmic ancilla register size $a = \lceil \log_2 m \rceil$ and v_k following the Gray code sequence (triangular markers), and with a linear ancilla register size $a = m$ and $v_k = 2^k$ (square markers).

5.2 Block Encoding of Operator A_4

Next, we consider the joint operator $A_4^{(1,2)}$, which is a linear combination of $A_1^{(1)}$ and $A_1^{(2)}$. As discussed in Section 4.5.4, we can use the same transformation operators T_k and phases γ_k for both $A_1^{(1)}$ and $A_1^{(2)}$. The resulting quantum circuit in Figure 3 only requires one application of U_{tag} , U_{tag}^\dagger and U_{correct} which leads to a decrease in the total two-qubit gate count and quantum circuit depth compared to the LCU approach as can be seen in Figure 5

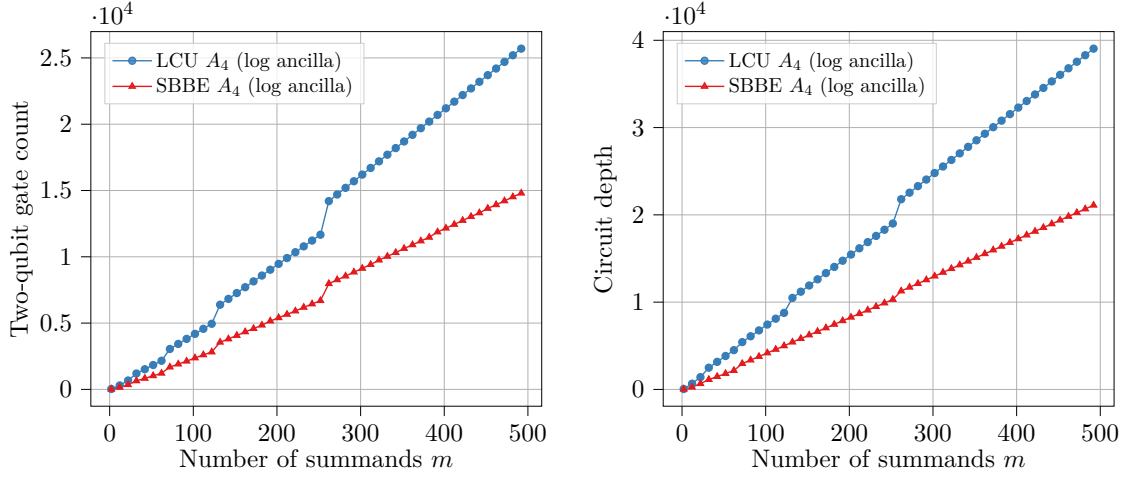


Figure 5: Numerical comparison of two-qubit gate count and quantum circuit depth for block encoding of the operator $A_4^{(1,2)}$ with the LCU method ($a = \lceil \log_2 m \rceil$) versus our proposed stabilizer-based block encoding (SBBE) with $a = \lceil \log_2(m) \rceil$ and v_k following the Gray code sequence.

5.3 Linear Ancilla Register

As already mentioned, our method can be easily extended to larger ancilla register sizes. We now want to show that extending to a linear ancilla register with $a = m$ qubits can significantly reduce the overall quantum circuit complexity. For the control states (see Figure 2), we choose $v_k = 2^k$. This has the property that the implementation of U_{correct} only requires single qubit controlled gates, see (60). The resulting quantum circuit implementation of U_{correct} can be seen in Figure 6. Again, we numerically investigate the

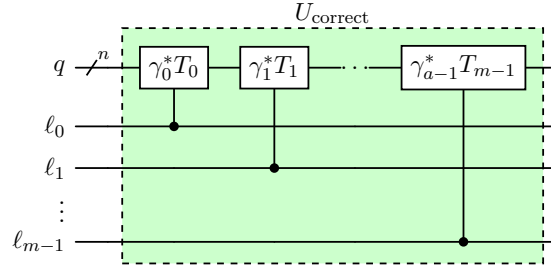


Figure 6: Quantum circuit of U_{correct} with $a = m$ and $v_k = 2^k$.

two-qubit gate count and the quantum circuit depth of the examples $A_1^{(1)}$, $A_2^{(1)}$, and $A_3^{(1)}$ and also plot the results in Figure 4 (square markers). We can observe a drastic reduction of quantum resources compared to the logarithmic case with our proposed method and LCU, although at the cost of a reduced success probability (see Section 3.2).

In this work, we only compare our proposed method to an LCU approach that uses a logarithmic-size ancilla register. It is worth noting that LCU can also be extended to larger ancilla registers, which can significantly reduce the overall quantum circuit complexity [25]. However, such extensions require modifications to the PREPARE and UNPREPARE oracles, which is not always straightforward, especially for cases between fully logarithmic and fully linear ancilla register sizes. In contrast, our method can be more easily adapted to ancilla registers of arbitrary size, potentially enabling better trade-offs between ancilla register size and circuit complexity. A detailed exploration of these intermediate regimes

and a comparison with LCU for various ancilla sizes are left for future work.

6 Conclusions

In this work, we introduced a novel block encoding scheme for implementing linear combinations of Pauli strings using the stabilizer formalism. Our approach transforms Pauli strings with commuting components into fully anti-commuting ones, enabling the direct implementation of their linear combinations as unitary operators, followed by a stabilizer-based correction step to recover the original operator. This method can be realized with an ancilla register scaling logarithmically with the number of Pauli strings, while also allowing straightforward extension to larger ancilla register sizes. We introduced four concrete examples and, through numerical simulations, compared the two-qubit gate complexity and circuit depth of our method with the Linear Combination of Unitaries (LCU) approach. For logarithmic ancilla register sizes, the complexity is comparable to LCU, with the potential for improvements beyond LCU if specific structures can be exploited. For linear ancilla register sizes, our method significantly reduces the overall quantum circuit complexity.

We emphasize again that the maximum number of pairwise anti-commuting Pauli strings is $2n + 1$ for an n qubit system [21]. Operators exceeding this limit can be implemented by introducing additional LCU steps to combine individually prepared block encodings. Combining these block encodings with LCU offers a path towards implementing full Hamiltonians for practical quantum simulations.

Furthermore, although this paper focused on operators with real coefficients for simplicity, the framework could also accommodate arbitrary complex coefficients by using general phase gates in the correction operator U_{correct} . A detailed exploration of this extension is reserved for future research.

Finally, it is crucial to note that the examples in this work are limited to block encodings of linear combinations where all Pauli strings commute. This restriction makes calculating the stabilizers more straightforward but can be seen as a worst-case scenario for the overall quantum circuit complexity of our proposed method. In many practical cases, some Pauli strings are already anti-commuting within the set. Our method would then require fewer corrections, potentially enhancing the efficiency beyond the examples analyzed here.

Acknowledgments

The authors thank Leon Rullkötter for carefully proofreading the manuscript and Thomas Wellens for valuable discussions.

This work was funded by the Ministry of Economic Affairs, Labour, and Tourism Baden-Württemberg within the Competence Center Quantum Computing Baden-Württemberg.

References

- [1] Guang Hao Low et al. “Optimal Hamiltonian simulation by quantum signal processing”. In: *Physical Review Letters* 118.1 (2017). ISSN: 1079-7114. DOI: [10.1103/physrevlett.118.010501](https://doi.org/10.1103/physrevlett.118.010501).
- [2] Guang Hao Low et al. “Hamiltonian simulation by qubitization”. In: *Quantum* 3 (2019), p. 163. ISSN: 2521-327X. DOI: [10.22331/q-2019-07-12-163](https://doi.org/10.22331/q-2019-07-12-163).

- [3] András Gilyén et al. “Quantum singular value transformation and beyond: exponential improvements for quantum matrix arithmetics”. In: *Proceedings of the 51st Annual ACM SIGACT Symposium on Theory of Computing*. STOC ’19. ACM, 2019, pp. 193–204. DOI: [10.1145/3313276.3316366](https://doi.org/10.1145/3313276.3316366).
- [4] John M. Martyn et al. “Grand unification of quantum algorithms”. In: *PRX Quantum* 2.4 (2021). ISSN: 2691-3399. DOI: [10.1103/prxquantum.2.040203](https://doi.org/10.1103/prxquantum.2.040203).
- [5] Andrew M. Childs et al. “Hamiltonian simulation using linear combinations of unitary operations”. In: *Quantum Information and Computation* 12 (2012). ISSN: 1533-7146. DOI: [10.26421/qic12.11-12](https://doi.org/10.26421/qic12.11-12).
- [6] Daan Camps et al. “Explicit quantum circuits for block encodings of certain sparse matrices”. In: *SIAM Journal on Matrix Analysis and Applications* 45.1 (2024), pp. 801–827. DOI: [10.1137/22M1484298](https://doi.org/10.1137/22M1484298).
- [7] Christoph Sünderhauf et al. “Block-encoding structured matrices for data input in quantum computing”. In: *Quantum* 8 (2024), p. 1226. ISSN: 2521-327X. DOI: [10.22331/q-2024-01-11-1226](https://doi.org/10.22331/q-2024-01-11-1226).
- [8] Andreas Sturm et al. “Efficient and explicit block encoding of finite difference discretizations of the Laplacian”. 2025. arXiv: [2509.02429 \[quant-ph\]](https://arxiv.org/abs/2509.02429).
- [9] Diyi Liu et al. “An efficient quantum circuit for block encoding a pairing Hamiltonian”. 2024. arXiv: [2402.11205 \[nucl-th\]](https://arxiv.org/abs/2402.11205).
- [10] Jiaqi Leng et al. “Expanding hardware-efficiently manipulable Hilbert space via Hamiltonian embedding”. In: *Quantum* 9 (2025), p. 1857. ISSN: 2521-327X. DOI: [10.22331/q-2025-09-11-1857](https://doi.org/10.22331/q-2025-09-11-1857).
- [11] Yuta Kikuchi et al. “Realization of quantum signal processing on a noisy quantum computer”. In: *npj Quantum Information* 9.1 (2023). ISSN: 2056-6387. DOI: [10.1038/s41534-023-00762-0](https://doi.org/10.1038/s41534-023-00762-0).
- [12] Leon Rullkötter et al. “Resource-efficient variational block-encoding”. 2025. arXiv: [2507.17658 \[quant-ph\]](https://arxiv.org/abs/2507.17658).
- [13] B. David Clader et al. “Quantum resources required to block-encode a matrix of classical data”. In: *IEEE Transactions on Quantum Engineering* 3 (2022), pp. 1–23. ISSN: 2689-1808. DOI: [10.1109/tqe.2022.3231194](https://doi.org/10.1109/tqe.2022.3231194).
- [14] Andrew Zhao et al. “Measurement reduction in variational quantum algorithms”. In: *Phys. Rev. A* 101 (6 2020), p. 062322. DOI: [10.1103/PhysRevA.101.062322](https://doi.org/10.1103/PhysRevA.101.062322).
- [15] Artur F. Izmaylov et al. “Unitary partitioning approach to the measurement problem in the Variational Quantum Eigensolver method”. In: *Journal of Chemical Theory and Computation* 16.1 (2020), pp. 190–195. DOI: [10.1021/acs.jctc.9b00791](https://doi.org/10.1021/acs.jctc.9b00791).
- [16] Robert A. Lang et al. “Unitary transformation of the electronic Hamiltonian with an exact quadratic truncation of the Baker-Campbell-Hausdorff expansion”. 2020. arXiv: [2002.05701 \[quant-ph\]](https://arxiv.org/abs/2002.05701).
- [17] Ilya G. Ryabinkin et al. “Efficient construction of involutory linear combinations of anti-commuting Pauli generators for large-scale iterative qubit coupled cluster calculations”. 2023. arXiv: [2301.10690 \[quant-ph\]](https://arxiv.org/abs/2301.10690).
- [18] Qi Zhao et al. “Exploiting anticommutation in Hamiltonian simulation”. In: *Quantum* 5 (2021), p. 534. ISSN: 2521-327X. DOI: [10.22331/q-2021-08-31-534](https://doi.org/10.22331/q-2021-08-31-534).
- [19] Daniel Gottesman. “Theory of fault-tolerant quantum computation”. In: *Physical Review A* 57.1 (1998), pp. 127–137. ISSN: 1050-2947. DOI: [10.1103/PhysRevA.57.127](https://doi.org/10.1103/PhysRevA.57.127).

- [20] Michael A. Nielsen et al. “Quantum computation and quantum information”. Cambridge University Press, 2000. ISBN: 9780521635035.
- [21] Rahul Sarkar et al. “On sets of commuting and anticommuting Paulis”. 2019. arXiv: [1909.08123 \[quant-ph\]](https://arxiv.org/abs/1909.08123).
- [22] Frank Gray. “Pulse code communication”. Patent US2632058. Granted Mar 17, 1953. 1953.
- [23] Pierre-Antoine Bernard et al. “Distinctive features of inhomogeneous spin chains”. 2025. arXiv: [2411.09487 \[quant-ph\]](https://arxiv.org/abs/2411.09487).
- [24] Ali Javadi-Abhari et al. “Quantum computing with Qiskit”. 2024. arXiv: [2405.08810 \[quant-ph\]](https://arxiv.org/abs/2405.08810).
- [25] Filippo Della Chiara et al. “Efficient LCU block encodings through Dicke states preparation”. 2025. arXiv: [2507.20887 \[quant-ph\]](https://arxiv.org/abs/2507.20887).
- [26] Eleanor Rieffel et al. “Quantum computing: a gentle introduction”. 1st. The MIT Press, 2011. ISBN: 9780262015066.
- [27] Olivia Di Matteo et al. “Improving Hamiltonian encodings with the Gray code”. In: *Phys. Rev. A* 103 (4 2021), p. 042405. DOI: [10.1103/PhysRevA.103.042405](https://doi.org/10.1103/PhysRevA.103.042405).
- [28] Maxime Remaud et al. “Ancilla-free quantum adder with sublinear depth”. In: *Reversible Computation*. Springer Nature Switzerland, 2025, pp. 137–154. ISBN: 9783031970634. DOI: [10.1007/978-3-031-97063-4_11](https://doi.org/10.1007/978-3-031-97063-4_11).
- [29] Elisa Bäumer et al. “Measurement-based long-range entangling gates in constant depth”. In: *Phys. Rev. Res.* 7 (2 2025), p. 023120. DOI: [10.1103/PhysRevResearch.7.023120](https://doi.org/10.1103/PhysRevResearch.7.023120).

A Proof of Main Theorem

In this appendix, we show that the quantum circuit shown in Figures 1 and 2 is indeed a block encoding of the matrix A given in (9a) as linear combination of m Pauli strings P_0, \dots, P_{m-1} . We start by introducing the following notation: For a Pauli string T that commutes with P_0, \dots, P_{m-1} according to

$$TP_k T = (-1)^{t^{(k)}} P_k, \quad t^{(k)} \in \{0, 1\}, \quad (35)$$

we call $t = (t^{(0)}, \dots, t^{(m-1)})$ the commutation vector of T . In the subsequence we show two auxiliary results needed for our main theorem. In the first, we prove that the condition (16) for the Pauli strings T_0, \dots, T_{m-1} of the circuit in Figure 2 guarantees that the transformed operators R_0, \dots, R_{m-1} , where $R_j = T_j P_j$, are anti-commuting.

Lemma 1. *Let T_0, \dots, T_{m-1} be commuting Pauli strings. Assume that their commutation vectors t_0, \dots, t_{m-1} with respect to the Pauli strings P_0, \dots, P_{m-1} satisfy*

$$t_i^{(k)} = \begin{cases} 1, & \text{if } i \leq k \text{ and } P_i P_k = P_k P_i, \\ 0, & \text{otherwise.} \end{cases} \quad (36)$$

Then, the transformed Pauli strings $R_j = T_j P_j$, $j = 0, \dots, m-1$, are mutually anti-commuting,

$$R_i R_j = -R_j R_i, \quad i, j = 0, 1, \dots, m-1, \quad i \neq j. \quad (37)$$

Proof. For $i < k$ and $P_i P_k = P_k P_i$ we have

$$R_i R_k = T_i P_i T_k P_k \stackrel{(36)}{=} T_i T_k P_i P_k = T_k T_i P_i P_k = T_k T_i P_k P_i \stackrel{(36)}{=} -T_k P_k T_i P_i = -R_k R_i. \quad (38)$$

The case $i > k$ and $P_i P_k = P_k P_i$ follows in a similar way. For the case $P_i P_k = -P_k P_i$ we have

$$R_i R_k = T_i P_i T_k P_k \stackrel{(36)}{=} T_i T_k P_i P_k = T_k T_i P_i P_k = -T_k T_i P_k P_i \stackrel{(36)}{=} -T_k P_k T_i P_i = -R_k R_i. \quad (39)$$

□

Note that the R_j themselves are not Pauli strings in the sense of (8) since they can have a phase. Factoring out the phase

$$\tilde{P}_j = \gamma_j R_j = \gamma_j T_j P_j, \quad \gamma_j \in \{\pm 1, \pm i\}, \quad (40)$$

gives Pauli strings $\tilde{P}_0, \dots, \tilde{P}_{m-1}$ with the same anti-commuting behavior as R_0, \dots, R_{m-1} . Also note that the T_i have the same commutation properties for \tilde{P}_k as for P_k :

$$T_i \tilde{P}_k = \gamma_k T_i T_k P_k = \gamma_k T_k T_i P_k = (-1)^{t_i^{(k)}} \gamma_k T_k P_k T_i = (-1)^{t_i^{(k)}} \tilde{P}_k T_i. \quad (41)$$

In the next lemma we show an identity for the Hadamard transformations that we use in the circuit in Figure 2. For this let us consider a register with a qubits. Any integer $v \in \{0, 1, \dots, 2^a - 1\}$ has a unique binary representation $v = v_0 v_1 \dots v_{a-1}$,

$$v = \sum_{k=0}^{a-1} v_k 2^{a-1-k}. \quad (42)$$

We will write \mathbf{v} when we mean the binary representation of v . For two integers $v, w \in \{0, 1, \dots, 2^a - 1\}$ we define

$$\Delta(v, w) = \mathbf{v} \cdot \mathbf{w} = d_{\text{Hamming}}(\mathbf{v} \wedge \mathbf{w}) = \text{number of common 1 bits}. \quad (43)$$

Lemma 2. For $v \in \{0, 1, \dots, 2^a - 1\}$ we have

$$H^{\otimes a} |v\rangle = \frac{1}{\sqrt{2^a}} \sum_{\ell=0}^{2^a-1} \prod_{\substack{i=0 \\ 1_i=1}}^{a-1} (-1)^{\Delta(2^{a-1-i}, v)} |\ell\rangle . \quad (44)$$

Proof. By definition of the Hadamard gate H , we have

$$H^{\otimes a} |v\rangle = \frac{1}{\sqrt{2^a}} \sum_{\ell=0}^{2^a-1} (-1)^{\Delta(\ell, v)} |\ell\rangle . \quad (45)$$

The binary representation of an integer $\ell \in \{0, 1, \dots, 2^a - 1\}$ can be written as

$$1 = \bigoplus_{\substack{i=0 \\ 1_i=1}}^{a-1} 2^{a-1-i} , \quad 2^{a-1-i} = \underbrace{0 \dots 0}_i \underbrace{1 0 \dots 0}_{a-1-i} , \quad (46)$$

where \oplus is the bitwise addition modulo 2. In [26] it is shown that for integers x, y , and z and associated bitstrings \mathbf{x}, \mathbf{y} , and \mathbf{z} it holds

$$(\mathbf{x} \oplus \mathbf{y}) \cdot \mathbf{z} =_2 \Delta(x, z) + \Delta(y, z) , \quad (47)$$

where $=_2$ denotes equality modulo 2. Combining the last two equations we obtain

$$\Delta(\ell, v) =_2 \sum_{\substack{i=0 \\ 1_i=1}}^{a-1} \Delta(2^{a-1-i}, v) . \quad (48)$$

Inserting this in (45) concludes the proof. \square

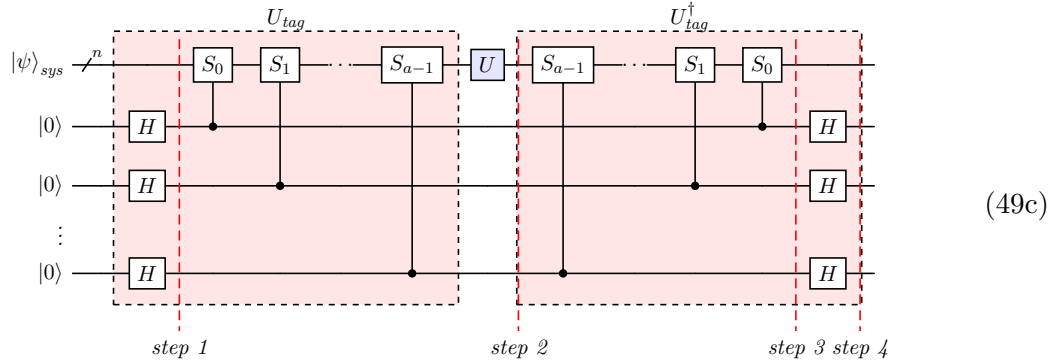
Theorem 1. Let T_0, \dots, T_{m-1} and R_0, \dots, R_{m-1} be the operators from Lemma 1 and $\tilde{P}_0, \dots, \tilde{P}_{m-1}$ be given by (40). Moreover, let U be given by

$$U = \sum_{k=0}^{m-1} \alpha_k \tilde{P}_k . \quad (49a)$$

Finally, let $v_0, \dots, v_{m-1} \in \{0, 1, \dots, 2^a - 1\}$ be integers and let S_0, \dots, S_{a-1} be Pauli strings with commuting vectors s_0, \dots, s_{a-1} that satisfy

$$s_i^{(k)} = \Delta(2^{a-1-i}, v_k) . \quad (49b)$$

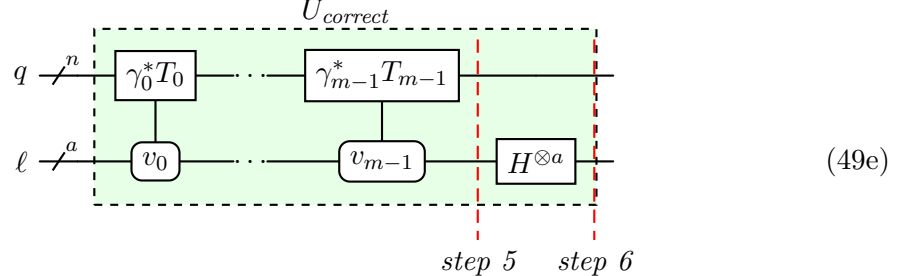
Then, the quantum circuit



generates the state

$$\sum_{k=0}^{m-1} \alpha_k \tilde{P}_k |\psi\rangle_{sys} |v_k\rangle_{anc} . \quad (49d)$$

Appending the quantum circuit (49c) with



gives the state

$$\frac{1}{\sqrt{2^a}} \sum_{k=0}^{m-1} \alpha_k P_k |\psi\rangle_{sys} |0\rangle_{anc} + |\perp\rangle . \quad (49f)$$

Consequently, the quantum circuit (49c) + (49e) is an exact block encoding of A in (9a) with $\lambda = \frac{1}{\sqrt{2^a}}$.

Proof. Note that by (41) and (49b) we have

$$S_i \tilde{P}_k S_i = (-1)^{\Delta(2^{a-1-i}, v_k)} \tilde{P}_k . \quad (50)$$

Going through the steps of the quantum circuit (49c) gives

$$\begin{aligned}
|\psi\rangle_{sys} |0\rangle_{anc} &\xrightarrow{\frac{1}{\sqrt{2^a}} \sum_{\ell=0}^{2^a-1} |\psi\rangle_{sys} |\ell\rangle_{anc}} \text{step 1} \\
&\xrightarrow{\frac{1}{\sqrt{2^a}} \sum_{\ell=0}^{2^a-1} U \prod_{\substack{i=0 \\ 1_i=1}}^{a-1} S_i |\psi\rangle_{sys} |\ell\rangle_{anc}} \text{step 2} \\
&= \frac{1}{\sqrt{2^a}} \sum_{\ell=0}^{2^a-1} \sum_{k=0}^{m-1} \alpha_k \tilde{P}_k \prod_{\substack{i=0 \\ 1_i=1}}^{a-1} S_i |\psi\rangle_{sys} |\ell\rangle_{anc} \\
&\stackrel{(50)}{=} \frac{1}{\sqrt{2^a}} \sum_{\ell=0}^{2^a-1} \sum_{k=0}^{m-1} \left(\prod_{\substack{i=0 \\ 1_i=1}}^{a-1} (-1)^{\Delta(2^{a-1-i}, v_k)} S_i \right) \alpha_k \tilde{P}_k |\psi\rangle_{sys} |\ell\rangle_{anc} \\
&\xrightarrow{\frac{1}{\sqrt{2^a}} \sum_{\ell=0}^{2^a-1} \sum_{k=0}^{m-1} \left(\prod_{\substack{i=0 \\ 1_i=1}}^{a-1} (-1)^{\Delta(2^{a-1-i}, v_k)} \right) \alpha_k \tilde{P}_k |\psi\rangle_{sys} |\ell\rangle_{anc}} \text{step 3} \\
&= \sum_{k=0}^{m-1} \alpha_k \tilde{P}_k |\psi\rangle_{sys} \frac{1}{\sqrt{2^a}} \sum_{\ell=0}^{2^a-1} \prod_{\substack{i=0 \\ 1_i=1}}^{a-1} (-1)^{\Delta(2^{a-1-i}, v_k)} |\ell\rangle_{anc} \\
&\stackrel{(44)}{=} \sum_{k=0}^{m-1} \alpha_k \tilde{P}_k |\psi\rangle_{sys} H^{\otimes a} |v_k\rangle_{anc} \\
&\xrightarrow{\sum_{k=0}^{m-1} \alpha_k \tilde{P}_k |\psi\rangle_{sys} |v_k\rangle_{anc}} \text{step 4}
\end{aligned}$$

This shows (49d). Applying (49e) further evolves the state as

$$\begin{aligned}
\sum_{k=0}^{m-1} \alpha_k \tilde{P}_k |\psi\rangle_{\text{sys}} |v_k\rangle_{\text{anc}} &\rightarrow \sum_{k=0}^{m-1} \alpha_k \gamma_k^* T_k \tilde{P}_k |\psi\rangle_{\text{sys}} |v_k\rangle_{\text{anc}} && \text{step 5} \\
&= \sum_{k=0}^{m-1} \alpha_k P_k |\psi\rangle_{\text{sys}} |v_k\rangle_{\text{anc}} \\
&\rightarrow \sum_{k=0}^{m-1} \alpha_k P_k |\psi\rangle_{\text{sys}} H^{\otimes a} |v_k\rangle_{\text{anc}} && \text{step 6} \\
&= \frac{1}{\sqrt{2^a}} \sum_{k=0}^{m-1} \alpha_k P_k |\psi\rangle_{\text{sys}} |0\rangle_{\text{anc}} + |\perp\rangle .
\end{aligned}$$

Here, we used (40) for the first equality and

$$H^{\otimes a} |v\rangle = \frac{1}{\sqrt{2^a}} \left(|0\rangle + \sum_{\ell=1}^{2^a-1} (-1)^{\Delta(\ell, v)} |\ell\rangle \right), \quad v \in \{0, 1, \dots, 2^a - 1\}, \quad (51)$$

for the second one. This concludes the proof. \square

B Construction of Stabilizers

In the next two lemmas we show that for every choice of commuting vectors s_0, \dots, s_{a-1} the Pauli strings S_0, \dots, S_{a-1} can be constructed from products of T_0, \dots, T_{m-1} . This means that the only requirement of Theorem 1 is the existence of T_0, \dots, T_{m-1} with the commuting property (36) of Lemma 1. To show this, let us denote with \mathcal{T} the set generated by T_0, \dots, T_{m-1} ,

$$\mathcal{T} = \langle T_0, \dots, T_{m-1} \rangle = \{ T_0^{r^{(0)}} T_1^{r^{(1)}} \dots T_{m-1}^{r^{(m-1)}} \mid r^{(0)}, r^{(1)}, \dots, r^{(m-1)} \in \{0, 1\} \}. \quad (52)$$

Lemma 3. *Let T_0, \dots, T_{m-1} be the Pauli strings from Lemma 1 and t_0, \dots, t_{m-1} be their commutation vectors. Moreover, let $M_{\mathcal{T}}$ be given by*

$$M_{\mathcal{T}} = (t_0 \ t_1 \ \dots \ t_{m-1}) = \begin{pmatrix} 1 & 0 & \dots & 0 \\ t_0^{(1)} & \ddots & \ddots & \vdots \\ \vdots & & \ddots & 0 \\ t_0^{(m-1)} & \dots & t_{m-2}^{(m-1)} & 1 \end{pmatrix}. \quad (53)$$

Then, the following holds:

- Let $T \in \mathcal{T}$ with $T = T_0^{r^{(0)}} T_1^{r^{(1)}} \dots T_{m-1}^{r^{(m-1)}}$ and denote $r = (r^{(0)}, \dots, r^{(m-1)})$. Then, the commuting vector t of T is given by

$$t = M_{\mathcal{T}} r = \begin{pmatrix} r^{(0)} \\ t_0^{(1)} r^{(0)} + r^{(1)} \\ \vdots \\ t_0^{(1)} r^{(0)} + t_1^{(1)} r^{(1)} + \dots + r^{(m-1)} \end{pmatrix}. \quad (54)$$

- Let $t = (t^{(0)}, t^{(1)}, \dots, t^{(m-1)}) \in \{0, 1\}^m$ be a vector. Then, there is a unique $T \in$

\mathcal{T} that has t as commuting vector. It is given by $T = T_0^{r(0)} T_1^{r(1)} \dots T_{m-1}^{r(m-1)}$ with $r = (r(0), \dots, r(m-1))$ defined by

$$r = M_{\mathcal{T}}^{-1}t. \quad (55)$$

All arithmetic is modulo 2.

Proof. For the first point, note that the commutation vector t for a product $T = T_k T_i$ is given by $t = t_k + t_i \pmod{2}$. The second claim follows because $M_{\mathcal{T}}$ is always invertible. This follows because it is a triangular matrix and thus its determinant equals the product of its diagonal entries $\det(M_{\mathcal{T}}) = 1$. \square

Note that Lemma 3 shows that \mathcal{T} is a stabilizer group. This follows from the fact that $-I$ has the commuting vector $(0, \dots, 0)$ but the unique element in \mathcal{T} with this commuting vector is given by $+I$.

B.1 Pairwise Commuting Pauli Strings

Next, we consider the special case where all Pauli strings P_0, \dots, P_{m-1} are pairwise commuting

$$P_i P_j = P_j P_i, \quad i, j = 0, \dots, m-1. \quad (56)$$

In this case, we have

$$M_{\mathcal{T}} = \begin{pmatrix} 1 & 0 & \dots & 0 \\ \vdots & \ddots & \ddots & \vdots \\ \vdots & & \ddots & 0 \\ 1 & \dots & \dots & 1 \end{pmatrix} \quad \text{and} \quad M_{\mathcal{T}}^{-1} = \begin{pmatrix} 1 & 0 & \dots & \dots & 0 \\ 1 & \ddots & \ddots & & \vdots \\ 0 & \ddots & \ddots & \ddots & \vdots \\ \vdots & \ddots & \ddots & \ddots & 0 \\ 0 & \dots & 0 & 1 & 1 \end{pmatrix}. \quad (57)$$

As a consequence, we have an explicit expression for (55) given by

$$r = M_{\mathcal{T}}^{-1}t = \begin{pmatrix} t^{(0)} \\ t^{(0)} + t^{(1)} \\ \vdots \\ t^{(m-2)} + t^{(m-1)} \end{pmatrix}. \quad (58)$$

This enables us to explicitly compute how the stabilizers S_0, \dots, S_{a-1} are constructed from T_0, \dots, T_{m-1} .

Lemma 4. *Let the Pauli strings P_0, \dots, P_{m-1} be pairwise commuting in the sense of (56). Additionally, let $v_0, \dots, v_{m-1} \in \{0, 1, \dots, 2^a - 1\}$ be integers and let S_0, \dots, S_{a-1} be Pauli strings with commuting vectors s_0, \dots, s_{a-1} that satisfy (49b). Then, we have*

$$S_i = T_0^{r_i^{(0)}} \dots T_{m-1}^{r_i^{(m-1)}}, \quad r_i^{(k)} = \begin{cases} 2^{a-1-i} \cdot (v_{k-1} \oplus v_k), & \text{if } k \geq 1, \\ 2^{a-1-i} \cdot v_0, & \text{if } k = 0. \end{cases} \quad (59)$$

Proof. The claim follows from (47) and (58). \square

We now discuss possible choices of the register size a and the integers v_0, \dots, v_{m-1} and what stabilizers S_0, \dots, S_{a-1} this induces. We begin with the two canonical choices.

Linear-size ancilla register For $a = m$, i.e. the number of ancillas a equal to the number of summands m in A , a possible choice for v_0, \dots, v_{m-1} is given by

$$v_k = 2^k, \quad \text{so that } \mathbf{v}_k = \underbrace{0 \dots 0}_{m-k-1} \underbrace{1 0 \dots 0}_k. \quad (60)$$

By Lemma 4 we obtain

$$r_0^{(k)} = \begin{cases} 1, & \text{if } k = a - 1, \\ 0, & \text{else,} \end{cases} \quad (61)$$

in the case $i = 0$ and

$$r_i^{(k)} = \begin{cases} 1, & \text{if } k \in \{a - i, a - i + 1\}, \\ 0, & \text{else,} \end{cases} \quad (62)$$

for $i \geq 1$. This translates to

$$S_0 = T_{m-1}, \quad S_i = T_{m-i} T_{m-i-1}, \text{ for } i \geq 1. \quad (63)$$

The resulting S_i for $m \leq 14$ can be seen in Table 1.

Logarithmic-size ancilla register We choose $a = \lceil \log_2 m \rceil$ and $v_k = k$. By Lemma 4 we obtain

$$r_i^{(k)} = \begin{cases} 1, & \text{if } k \pmod{2^{a-1-i}} = 0, \\ 0, & \text{else.} \end{cases} \quad (64)$$

This gives the stabilizers

$$\begin{aligned} S_0 &= T_{2^{a-1}}, \\ S_1 &= T_{2^{a-2}} T_{2 \cdot 2^{a-2}}, \\ S_2 &= T_{2^{a-3}} T_{2 \cdot 2^{a-3}} T_{3 \cdot 2^{a-3}} T_{4 \cdot 2^{a-3}}, \\ &\dots \\ S_{m-1} &= T_{2^0} T_{2 \cdot 2^0} T_{3 \cdot 2^0} \dots T_{(a-1) \cdot 2^0}. \end{aligned} \quad (65)$$

The resulting S_i for $m \leq 14$ can be seen in Table 2.

Linear-minus-one-size ancilla register Here, we have $a = m - 1$ and the v_0, \dots, v_{m-1} are defined via their binary representation

$$\mathbf{v}_k = \underbrace{1 \dots 1}_k \underbrace{0 \dots 0}_{m-1-k}. \quad (66)$$

Since $\mathbf{v}_{k-1} \oplus \mathbf{v}_k = 2^{a-k}$ we obtain from Lemma 4

$$r_i^{(k)} = \begin{cases} 1, & \text{if } k = i + 1, \\ 0, & \text{else.} \end{cases} \quad (67)$$

Thus, we have

$$S_i = T_{i+1}. \quad (68)$$

The resulting S_i for $m \leq 14$ can be seen in Table 3.

Logarithmic-size ancilla register with Gray code Another possible choice with $a = \lceil \log_2 m \rceil$ is to use v_k of the Gray code, which is a binary numeral system in which two successive values differ in only one bit [22]. This property can be useful for quantum circuits, as Gray code sequences minimize the number of qubits that change state at each step, reducing the circuit complexity and error rates [27]. For example for $a = 3$ we have

$$v_0 = 000, v_1 = 001, v_2 = 011, v_3 = 010, v_4 = 110, v_5 = 111, v_6 = 101, v_7 = 100. \quad (69)$$

For this example we calculated the S_i numerically, see Table 4.

C Quantum Circuit Implementations

In this part of the appendix we show an efficient implementation of the unitaries $U^{(a,b)}$ used in the examples. Without loss of generality, we choose the number of Pauli strings m equal to the number of system qubits n . Let us recall that these unitaries are of the form

$$U^{(a,b)} = \sum_{k=0}^{m-1} \alpha_k \tilde{P}_k, \quad (70a)$$

with

$$\tilde{P}_0 = \sigma_0^{(b)}, \quad \tilde{P}_k = \left(\prod_{i=0}^{k-1} \sigma_i^{(a)} \right) \sigma_k^{(b)}, \quad k = 1, \dots, m-1, \quad (70b)$$

where $a, b \in \{1, 2, 3\}$, with $a \neq b$.

Lemma 5. *Let $a, b \in \{1, 2, 3\}$ with $a \neq b$ and let $c \in \{1, 2, 3\} \setminus \{a, b\}$. Moreover, let*

$$C_i^{(c,b)}(\theta) = \frac{1}{2}(I + \sigma^{(c)})_i + \frac{1}{2}(I - \sigma^{(c)})_i R \sigma_{i+1}^{(b)}(\theta). \quad (71)$$

Then, the quantum circuit in Figure 7 implements $U^{(a,b)}$ in (70a) with coefficients α_k given by

$$\alpha_k = \mu^k \prod_{i=0}^{k-1} \sin \frac{\theta_i}{2} \cos \frac{\theta_k}{2}, \quad k \in \{0, \dots, n-2\}, \quad \alpha_{n-1} = \mu^{n-1} \prod_{i=0}^{n-2} \sin \frac{\theta_i}{2}, \quad (72)$$

where $\mu = -i\gamma(c, b) \in \{\pm 1\}$.

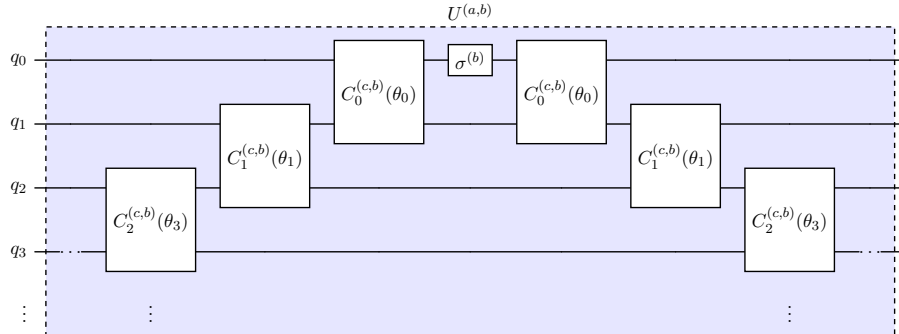


Figure 7: Quantum circuit implementation of operator $U^{(a,b)}$.

Note that for $c = 3$ the unitary $C_i^{(3,b)}(\theta)$ corresponds to a controlled $\sigma^{(b)}$ rotation,

$$C_i^{(3,b)}(\theta) = CR\sigma_{i,i+1}^{(b)}(\theta). \quad (73)$$

Proof. Using (3), (4), and the fact that $\sigma_i^{(b)}$ and $\sigma_i^{(c)}$ anti-commute we obtain

$$C_i^{(c,b)}(-\theta_i) \sigma_i^{(b)} C_i^{(c,b)}(\theta_i) = \cos \frac{\theta_i}{2} \sigma_i^{(b)} + \mu \sin \frac{\theta_i}{2} \sigma_i^{(a)} \sigma_{i+1}^{(b)}. \quad (74)$$

Since $C_{i+1}^{(c,b)}(\theta_{i+1})$ commutes with $\sigma_i^{(a)}$ and $\sigma_i^{(b)}$ we obtain

$$\begin{aligned} & C_{i+1}^{(c,b)}(-\theta_{i+1}) C_i^{(c,b)}(-\theta_i) \sigma_i^{(b)} C_i^{(c,b)}(\theta_i) C_{i+1}^{(c,b)}(\theta_{i+1}) \\ &= \cos \frac{\theta_i}{2} \sigma_i^{(b)} + \mu \sin \frac{\theta_i}{2} \sigma_i^{(a)} C_{i+1}^{(c,b)}(-\theta_{i+1}) \sigma_{i+1}^{(b)} C_{i+1}^{(c,b)}(\theta_{i+1}) \\ &= \cos \frac{\theta_i}{2} \sigma_i^{(b)} + \mu \sin \frac{\theta_i}{2} \sigma_i^{(a)} \left(\cos \frac{\theta_{i+1}}{2} \sigma_{i+1}^{(b)} + \mu \sin \frac{\theta_{i+1}}{2} \sigma_{i+1}^{(a)} \sigma_{i+2}^{(b)} \right) \\ &= \cos \frac{\theta_i}{2} \sigma_i^{(b)} + \mu \sin \frac{\theta_i}{2} \cos \frac{\theta_{i+1}}{2} \sigma_i^{(a)} \sigma_{i+1}^{(b)} + \mu^2 \sin \frac{\theta_i}{2} \sin \frac{\theta_{i+1}}{2} \sigma_i^{(a)} \sigma_{i+1}^{(a)} \sigma_{i+2}^{(b)}. \end{aligned}$$

Starting at $i = 0$ and iterating the upper calculation shows the claim. \square

D CNOT Fan-out

In this appendix, we discuss how multi-target controlled- $\sigma^{(1)}$ gates can be simplified using the concept of CNOT fan-out. For the decomposition of multi-target $\sigma^{(1)}$ operations, we use the quantum circuit shown in Figure 8. It can be seen that a t -target, c -controlled

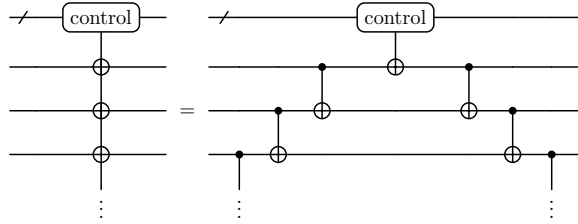


Figure 8: CNOT fan-out decomposition schematic.

$\sigma^{(1)}$ gate can be decomposed into $2(t - 1)$ single controlled $\sigma^{(1)}$ gates and one c -controlled $\sigma^{(1)}$ gate. Although such methods are not explored further in this work, the CNOT fan-out operation can be implemented with logarithmic circuit depth [28] and no additional ancillas. Moreover, if mid-circuit measurements are allowed, the fan-out can even be realized in constant depth using n ancilla qubits [29].

m	a	S_i
2	2	$S_0 = T_1; S_1 = T_0T_1$
3	3	$S_0 = T_2; S_1 = T_1T_2; S_2 = T_0T_1$
4	4	$S_0 = T_3; S_1 = T_2T_3; S_2 = T_1T_2; S_3 = T_0T_1$
5	5	$S_0 = T_4; S_1 = T_3T_4; S_2 = T_2T_3; S_3 = T_1T_2; S_4 = T_0T_1$
6	6	$S_0 = T_5; S_1 = T_4T_5; S_2 = T_3T_4; S_3 = T_2T_3; S_4 = T_1T_2; S_5 = T_0T_1$
7	7	$S_0 = T_6; S_1 = T_5T_6; S_2 = T_4T_5; S_3 = T_3T_4; S_4 = T_2T_3; S_5 = T_1T_2; S_6 = T_0T_1$
8	8	$S_0 = T_7; S_1 = T_6T_7; S_2 = T_5T_6; S_3 = T_4T_5; S_4 = T_3T_4; S_5 = T_2T_3; S_6 = T_1T_2; S_7 = T_0T_1$
9	9	$S_0 = T_8; S_1 = T_7T_8; S_2 = T_6T_7; S_3 = T_5T_6; S_4 = T_4T_5; S_5 = T_3T_4; S_6 = T_2T_3; S_7 = T_1T_2; S_8 = T_0T_1$
10	10	$S_0 = T_9; S_1 = T_8T_9; S_2 = T_7T_8; S_3 = T_6T_7; S_4 = T_5T_6; S_5 = T_4T_5; S_6 = T_3T_4; S_7 = T_2T_3; S_8 = T_1T_2; S_9 = T_0T_1$
11	11	$S_0 = T_{10}; S_1 = T_9T_{10}; S_2 = T_8T_9; S_3 = T_7T_8; S_4 = T_6T_7; S_5 = T_5T_6; S_6 = T_4T_5; S_7 = T_3T_4; S_8 = T_2T_3; S_9 = T_1T_2; S_{10} = T_0T_1$
12	12	$S_0 = T_{11}; S_1 = T_{10}T_{11}; S_2 = T_9T_{10}; S_3 = T_8T_9; S_4 = T_7T_8; S_5 = T_6T_7; S_6 = T_5T_6; S_7 = T_4T_5; S_8 = T_3T_4; S_9 = T_2T_3; S_{10} = T_1T_2; S_{11} = T_0T_1$
13	13	$S_0 = T_{12}; S_1 = T_{11}T_{12}; S_2 = T_{10}T_{11}; S_3 = T_9T_{10}; S_4 = T_8T_9; S_5 = T_7T_8; S_6 = T_6T_7; S_7 = T_5T_6; S_8 = T_4T_5; S_9 = T_3T_4; S_{10} = T_2T_3; S_{11} = T_1T_2; S_{12} = T_0T_1$
14	14	$S_0 = T_{13}; S_1 = T_{12}T_{13}; S_2 = T_{11}T_{12}; S_3 = T_{10}T_{11}; S_4 = T_9T_{10}; S_5 = T_8T_9; S_6 = T_7T_8; S_7 = T_6T_7; S_8 = T_5T_6; S_9 = T_4T_5; S_{10} = T_3T_4; S_{11} = T_2T_3; S_{12} = T_1T_2; S_{13} = T_0T_1$

Table 1: Stabilizers S_i for linear-size ancilla register (63).

m	a	S_i
2	1	$S_0 = T_1$
3	2	$S_0 = T_2; S_1 = T_1T_2$
4	2	$S_0 = T_2; S_1 = T_1T_2T_3$
5	3	$S_0 = T_4; S_1 = T_2T_4; S_2 = T_1T_2T_3T_4$
6	3	$S_0 = T_4; S_1 = T_2T_4; S_2 = T_1T_2T_3T_4T_5$
7	3	$S_0 = T_4; S_1 = T_2T_4T_6; S_2 = T_1T_2T_3T_4T_5T_6$
8	3	$S_0 = T_4; S_1 = T_2T_4T_6; S_2 = T_1T_2T_3T_4T_5T_6T_7$
9	4	$S_0 = T_8; S_1 = T_4T_8; S_2 = T_2T_4T_6T_8; S_3 = T_1T_2T_3T_4T_5T_6T_7T_8$
10	4	$S_0 = T_8; S_1 = T_4T_8; S_2 = T_2T_4T_6T_8; S_3 = T_1T_2T_3T_4T_5T_6T_7T_8T_9$
11	4	$S_0 = T_8; S_1 = T_4T_8; S_2 = T_2T_4T_6T_8T_{10}; S_3 = T_1T_2T_3T_4T_5T_6T_7T_8T_9T_{10}$
12	4	$S_0 = T_8; S_1 = T_4T_8; S_2 = T_2T_4T_6T_8T_{10}; S_3 = T_1T_2T_3T_4T_5T_6T_7T_8T_9T_{10}T_{11}$
13	4	$S_0 = T_8; S_1 = T_4T_8T_{12}; S_2 = T_2T_4T_6T_8T_{10}T_{12}; S_3 = T_1T_2T_3T_4T_5T_6T_7T_8T_9T_{10}T_{11}T_{12}$
14	4	$S_0 = T_8; S_1 = T_4T_8T_{12}; S_2 = T_2T_4T_6T_8T_{10}T_{12}; S_3 = T_1T_2T_3T_4T_5T_6T_7T_8T_9T_{10}T_{11}T_{12}T_{13}$

Table 2: Stabilizers S_i for logarithmic-size ancilla register (65).

m	a	S_i
2	1	$S_0 = T_1$
3	2	$S_0 = T_1; S_1 = T_2$
4	3	$S_0 = T_1; S_1 = T_2; S_2 = T_3$
5	4	$S_0 = T_1; S_1 = T_2; S_2 = T_3; S_3 = T_4$
6	5	$S_0 = T_1; S_1 = T_2; S_2 = T_3; S_3 = T_4; S_4 = T_5$
7	6	$S_0 = T_1; S_1 = T_2; S_2 = T_3; S_3 = T_4; S_4 = T_5; S_5 = T_6$
8	7	$S_0 = T_1; S_1 = T_2; S_2 = T_3; S_3 = T_4; S_4 = T_5; S_5 = T_6; S_6 = T_7$
9	8	$S_0 = T_1; S_1 = T_2; S_2 = T_3; S_3 = T_4; S_4 = T_5; S_5 = T_6; S_6 = T_7; S_7 = T_8$
10	9	$S_0 = T_1; S_1 = T_2; S_2 = T_3; S_3 = T_4; S_4 = T_5; S_5 = T_6; S_6 = T_7; S_7 = T_8; S_8 = T_9$
11	10	$S_0 = T_1; S_1 = T_2; S_2 = T_3; S_3 = T_4; S_4 = T_5; S_5 = T_6; S_6 = T_7; S_7 = T_8; S_8 = T_9; S_9 = T_{10}$
12	11	$S_0 = T_1; S_1 = T_2; S_2 = T_3; S_3 = T_4; S_4 = T_5; S_5 = T_6; S_6 = T_7; S_7 = T_8; S_8 = T_9; S_9 = T_{10}; S_{10} = T_{11}$
13	12	$S_0 = T_1; S_1 = T_2; S_2 = T_3; S_3 = T_4; S_4 = T_5; S_5 = T_6; S_6 = T_7; S_7 = T_8; S_8 = T_9; S_9 = T_{10}; S_{10} = T_{11}; S_{11} = T_{12}$
14	13	$S_0 = T_1; S_1 = T_2; S_2 = T_3; S_3 = T_4; S_4 = T_5; S_5 = T_6; S_6 = T_7; S_7 = T_8; S_8 = T_9; S_9 = T_{10}; S_{10} = T_{11}; S_{11} = T_{12}; S_{12} = T_{13}$

Table 3: Stabilizers S_i for linear-minus-one-size ancilla register (68).

m	a	S_i
2	1	$S_0 = T_1$
3	2	$S_0 = T_2; S_1 = T_1$
4	2	$S_0 = T_2; S_1 = T_1 T_3$
5	3	$S_0 = T_4; S_1 = T_2; S_2 = T_1 T_3$
6	3	$S_0 = T_4; S_1 = T_2; S_2 = T_1 T_3 T_5$
7	3	$S_0 = T_4; S_1 = T_2 T_6; S_2 = T_1 T_3 T_5$
8	3	$S_0 = T_4; S_1 = T_2 T_6; S_2 = T_1 T_3 T_5 T_7$
9	4	$S_0 = T_8; S_1 = T_4; S_2 = T_2 T_6; S_3 = T_1 T_3 T_5 T_7$
10	4	$S_0 = T_8; S_1 = T_4; S_2 = T_2 T_6; S_3 = T_1 T_3 T_5 T_7 T_9$
11	4	$S_0 = T_8; S_1 = T_4; S_2 = T_2 T_6 T_{10}; S_3 = T_1 T_3 T_5 T_7 T_9$
12	4	$S_0 = T_8; S_1 = T_4; S_2 = T_2 T_6 T_{10}; S_3 = T_1 T_3 T_5 T_7 T_9 T_{11}$
13	4	$S_0 = T_8; S_1 = T_4 T_{12}; S_2 = T_2 T_6 T_{10}; S_3 = T_1 T_3 T_5 T_7 T_9 T_{11}$
14	4	$S_0 = T_8; S_1 = T_4 T_{12}; S_2 = T_2 T_6 T_{10}; S_3 = T_1 T_3 T_5 T_7 T_9 T_{11} T_{13}$

Table 4: Stabilizers S_i for logarithmic-size ancilla register with Gray code sequence.